

A COHERENT TIMING SOLUTION FOR THE NEARBY ISOLATED NEUTRON STAR  
RX J1308.6+2127/RBS 1223D. L. KAPLAN<sup>1</sup> AND M. H. VAN KERKWIJK<sup>2</sup>*ApJ Letters in Press*

## ABSTRACT

We present a phase-connected timing solution for the nearby isolated neutron star RX J1308.6+2127 (RBS 1223). From dedicated *Chandra* observations as well as archival *Chandra* and *XMM-Newton* data spanning a period of five years, we demonstrate that the 10.31-sec pulsations are slowing down steadily at a rate of  $\dot{P} = 1.120(3) \times 10^{-13} \text{ s s}^{-1}$ . Under the assumption that this is due to magnetic dipole torques, we infer a characteristic age of 1.5 Myr and a magnetic field strength of  $3.4 \times 10^{13} \text{ G}$ . As with RX J0720.4–3125, the only other radio-quiet thermally emitting isolated neutron star for which a timing solution has been derived, the field strength is roughly consistent with what was inferred earlier from the presence of a strong absorption feature in its X-ray spectrum. Furthermore, for both sources the characteristic age is in excess of the cooling age inferred from standard cooling models. The sources differ, however, in their timing noise: while RX J0720.4–3125 showed considerable timing noise, RX J1308.6+2127 appears relatively stable.

*Subject headings:* pulsars: individual (RX J1308.6+2127) — stars: neutron — X-rays: stars

## 1. INTRODUCTION

The sample of nearby, radio-quiet, isolated neutron stars discovered by *ROSAT* (for a review, e.g., Haberl 2004) is of particular interest because of the unambiguous presence of strong, broad absorption features in the X-ray spectra of most sources. Since the spectra appear thermal, these features almost certainly arise in the neutron-star atmospheres. The features have usually been interpreted under the assumption of a pure hydrogen composition (not unlikely, given the short settling times for neutron stars) and a strong magnetic field (as suggested by the long, 3–10 s spin periods; Heyl & Hernquist 1998), with the absorption reflecting either the proton cyclotron line or transitions between bound states of neutral hydrogen (e.g., Haberl et al. 2003; van Kerkwijk et al. 2004).

In order to help determine the nature of the absorption features, as well as to elucidate what sets the isolated neutron stars apart from young rotation-powered pulsars, we have started a program to obtain phase-connected timing solutions, and use these to estimate ages and magnetic field strengths. Earlier, we presented our first results, for RX J0720.4–3125 (Kaplan & van Kerkwijk 2005); here, we consider a second source, RX J1308.6+2127.

RX J1308.6+2127 (also known as RBS 1223 and 1RXS J130848.6+212708) was identified as a possible nearby isolated neutron star by Schwpo et al. (1999). The identification was confirmed with the detection of a 5.16-s X-ray periodicity (Hambaryan et al. 2002) and a very faint ( $V \approx 28$  mag) probable optical counterpart with no radio emission

<sup>1</sup> Pappalardo Fellow; MIT Kavli Institute for Astrophysics and Space Research, Massachusetts Institute of Technology, 77 Massachusetts Avenue, 37-664D, Cambridge, MA 02139, USA; dlk@space.mit.edu

<sup>2</sup> Department of Astronomy and Astrophysics, University of Toronto, 60 St. George Street, Toronto, ON M5S 3H8, Canada; mhvk@astro.utoronto.ca

(Kaplan, Kulkarni, & van Kerkwijk 2002a). By comparing the periods measured from *Chandra* and archival *ROSAT* data, Hambaryan et al. (2002) inferred a spin-down rate of  $\dot{P} = (0.7 - 2.0) \times 10^{-11} \text{ s s}^{-1}$ , implying a very strong magnetic field of  $\gtrsim 10^{14} \text{ G}$ . Haberl (2004), however, showed that the 5.16-s periodicity was in fact the first harmonic, implying a true period of 10.31 s (see also Haberl et al. 2003), and that the spin-down rate inferred earlier was likely erroneous. This was confirmed by Schwpo et al. (2005), who attempted to determine a phase-connected timing solution, but failed due to cycle-count ambiguities.

Here, we show that with additional *Chandra* observations specifically obtained for timing purposes, we can obtain an unambiguous timing solution. We describe our analysis of the *Chandra* data, as well as of archival *ROSAT*, *Chandra*, and *XMM-Newton* data, in § 2, and use these to obtain a timing solution in § 3. Since our analysis closely follows the one used for RX J0720.4–3125 (Kaplan & van Kerkwijk 2005), we focus primarily on those aspects of the analysis that differ. We discuss the implications of our result in § 4.

## 2. OBSERVATIONS

Our primary data are eight observations taken with the Advanced CCD Imaging Spectrometer (ACIS; Garmire et al. 2003) aboard the *Chandra X-ray Observatory* (CXO). These were designed for timing accuracy, consisting of two sets of four exposures in the Continuous-Clocking (CC) mode geometrically spaced over a period of about two weeks and separated by about half a year. We combined these with data from other *Chandra* observations, as well as from observations with *XMM-Newton* and *ROSAT*. A log of all observations<sup>3</sup> is given in Table 1.

For the *Chandra* data, we processed the level-1

<sup>3</sup> We do not use data from *ROSAT* observation 703848, since we, like Hambaryan et al. (2002) and Schwpo et al. (2005), found there were insufficient counts to extract a period or an arrival time.

TABLE 1  
LOG OF OBSERVATIONS AND TIMES OF ARRIVAL

Instrument <sup>a</sup>	ID <sup>b</sup>	Date	Exp. (ks)	Counts	TOA <sup>c</sup> (MJD)
HRI .....	704082	1998 Oct 01	4.8	498	50824.2143496(30)
ACIS 1/8 ...	731	2000 Jun 24	9.5	7395	51719.5182790(5)
PN/sw .....	377-U2	2001 Dec 31	18.0	10633	52274.2594926(10)
PN/ff .....	561-S5	2003 Jan 01	27.0	66219	52640.4325929(5)
MOS1 .....	561-S3	2003 Jan 01	29.0	14469	52640.4265055(9)
MOS2 .....	561-S4	2003 Jan 01	29.0	14925	52640.4265042(7)
PN/ff .....	743-S3	2003 Dec 30	30.0	74587	53003.4668264(6)
MOS1 .....	743-S1	2003 Dec 30	32.0	16086	53003.4607372(7)
MOS2 .....	743-S2	2003 Dec 30	32.0	16523	53003.4607388(9)
HRC .....	4595	2004 Mar 30	90.1	33823	53095.3847872(16)
ACIS CC ...	5522	2005 Feb 14	16.0	8953	53415.6878535(10)
	5523	2005 Feb 15	5.7	3254	53416.5968822(17)
	5524	2005 Feb 19	5.2	2922	53420.1717683(14)
	5525	2005 Mar 10	5.6	2923	53439.0475044(11)
ACIS CC ...	5526	2005 Jul 09	15.1	7684	53560.2591584(8)
	5527	2005 Jul 10	5.1	2876	53561.2549594(17)
	5528	2005 Jul 14	5.2	2937	53565.7697939(18)
	5529	2005 Jul 29	5.2	3048	53580.7839447(14)

<sup>a</sup>HRI: High-Resolution Imager (Zombeck et al. 1995) aboard *ROSAT*. PN: *XMM-Newton*'s European Photon Imaging Camera with PN detectors (Strüder et al. 2001), used in full-frame (ff) or small window (sw) mode, with thin filter. MOS1/2: European Photon Imaging Cameras with MOS detectors aboard *XMM-Newton* (Turner et al. 2001), used in small-window mode with thin filter. HRC: High-Resolution Camera for spectroscopy aboard *Chandra* (HRC-S; Kraft et al. 1997), used with the Low-Energy Transmission Grating (LETG). ACIS: *Chandra*'s Advanced CCD Imaging Spectrometer, with the S3 chip used either in 1/8-subarray or in Continuous Clocking (CC) mode.

<sup>b</sup>Observation identifier (*CXO*, *ROSAT*) or revolution number and exposure identifier (*XMM-Newton*).

<sup>c</sup>The TOA is defined as the time of maximum light of the pulsation after the deepest minimum closest to the middle of each observation, and is given with  $1-\sigma$  uncertainties.

event lists to the level-2 stage following standard procedures and the latest calibration set (CALDB version 3.1.0). For the ACIS data, we extracted events within  $1''$  of the source with energies between 0.2 and 2.0 keV, and then applied a clock correction of 284.7  $\mu$ s (Davis, Holmes, & Myers 2003). For the HRC-S/LETG data, we extracted zeroth-order events from a circle with radius of  $1.^{\prime}3$ , and first-order events using the standard LETG spectral extraction windows, but limited to  $10\text{ \AA} \leq \lambda \leq 65\text{ \AA}$ . Finally, we used the **axbary** program to barycenter all of the events (using the X-ray position:  $\alpha_{\text{J}2000} = 13^{\text{h}}08^{\text{m}}48.^{\text{s}}27$ ,  $\delta_{\text{J}2000} = +21^{\circ}27'06.^{\prime}8$ ; Kaplan et al. 2002a)

For the *XMM-Newton* data, we used the standard procedures **emchain** and **epchain** (XMMSAS version 6.5.0) to reprocess the observations. Next, we extracted events within  $37.^{\prime}5$  of the source position (using standard quality and pattern selections) with energies from 0.12 keV to 1.2 keV, and used **barycen** to convert the arrival times to the solar-system barycenter. And finally, for the *ROSAT* HRI data, we extracted the events within  $12.^{\prime}5$  of the source. We barycentered these using the **FTOOLS** programs **ABC** and **BCT**, and converted the event times from Coordinated Universal Time (UTC) to Barycentric Dynamical Time (TDB) using the corrections supplied in Cox (2000, p. 14).

### 3. TIMING ANALYSIS

Our goal is to use times-of-arrival (TOAs) to infer a phase-coherent timing solution in which each cycle of the source is accounted for. To measure TOAs, we need an initial reference period. We determined this from the ACIS CC data-sets using a  $Z_2^2$  test (Buccheri et al. 1983), which combines power from the 10.31-s fundamental with

that from the 5.16-s harmonic (we could not detect significant power in any higher harmonics). We calculated  $Z_2^2$  both for the individual sets of four observations (observations 5522–5525 and 5526–5529) as well as for the eight observations combined. The overall  $Z_2^2$  spectrum has a single, well-defined peak, and all possible aliases are at considerably lower significances. The measured period is  $P = 10.31252293(9)$  s (here and below, numbers in parentheses indicate the formal  $1-\sigma$  uncertainties in the last digit unless otherwise indicated).

Using the period derived above, we constructed binned light curves (with 16 phase bins) for all of the observations. Unlike RX J0720.4–3125, RX J1308.6+2127 has non-sinusoidal pulsations and hence determining TOAs by fitting a single sinusoid would be inappropriate. Instead we fit for both the first harmonic and fundamental, with a possible phase shift between them:

$$N_i = A [\sin(2\pi(f_0 t_i + \phi_0)) + r_2 \sin(4\pi(f_0 t_i + \phi_0 + \Delta\phi_2))] + C, \quad (1)$$

where  $N_i$  is the number of counts in bin  $i$ ,  $f_0 = 0.096969481$  Hz is the frequency of the fundamental from above,  $t_i$  the time of bin  $i$  on the interval  $[0, P]$ , and the parameters are amplitude  $A$ , phase  $\phi_0$ , amplitude ratio  $r_2$ , phase offset  $\Delta\phi_2$ , and constant offset  $C$ . As can be seen in Figure 1, this model provides a good fit to even the highest-quality lightcurves, which are those derived from the long EPIC-PN observations. The inferred phase offset and relative amplitude are similar for both observations, with  $\Delta\phi_2 \approx 0.03$ , and  $r_2 \approx 2.8$ .

Assuming that the pulse profile is not varying, we measured arrival times for all of the data using the above model, but with  $\Delta\phi_2$  and  $r_2$  fixed at 0.03 and 2.8, respectively, which generally provides a good fit to the light curves (see Fig. 1 for the EPIC-PN data). Our

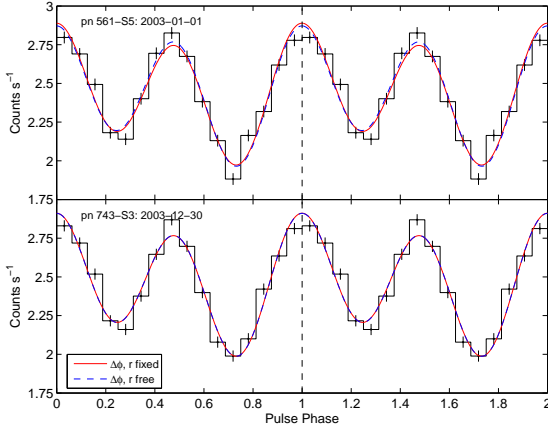


FIG. 1.— Pulse profiles of the two long EPIC-PN observations, showing the different fits to the binned lightcurves. Top: data from revolution 561; bottom: data from revolution 743. The solid red lines show the fits using Eqn. 1 with  $\Delta\phi_2$  and  $r_2$  free, while the dashed blue lines (largely indistinguishable from the red lines) show the fits with  $\Delta\phi_2$  and  $r_2$  fixed to the average best-fit values of 0.03 and 2.8. The zero point in phase has been chosen such that it coincides with the maximum following the deepest minimum, which we define as the reference position for the TOAs; it is indicated by the vertical dashed line at phase 0.

resulting arrival times are listed in Table 1. Here, we assigned these times to the time of the maximum of the model lightcurve that follows the lowest minimum and is nearest to the middle of the observation (see Fig. 1; this is the spectrally harder maximum from Schworer et al. 2005). For completeness, we note that the TOAs derived using the above model are consistent with those one would find using a simpler model consisting of only the first harmonic (i.e., a sinusoid at  $P = 5.16$  s): the mean absolute difference is  $0.2\sigma$ .

We determined a timing solution from the TOAs using an iterative procedure, as in Kaplan & van Kerkwijk (2005). We started with the *Chandra* ACIS CC TOAs and found that we were able to fit these without the need for a frequency derivative and with no cycle ambiguity, consistent with the power spectrum analysis. However, between the first ACIS CC TOA and the preceding TOA (*Chandra* HRC) there is a gap of 320 days and we found that a constant-frequency model led to a poor fit ( $\chi^2 = 202.7$  for 7 degrees of freedom). Including a frequency derivative  $\dot{\nu}$ , the cycle count over the gap became ambiguous by  $\pm 1$  cycle. The three possibilities—2683550, 2683551, and 2683552 cycles—lead to three possible solutions for  $\dot{\nu}$ :  $2.1 \times 10^{-15}$  Hz s $^{-1}$ ,  $1.0 \times 10^{-15}$  Hz s $^{-1}$ , and  $-1.1 \times 10^{-15}$  Hz s $^{-1}$ . Fortunately, the addition of the remaining data eliminates the first two of those solutions: with the *XMM-Newton* TOAs (and the remaining ACIS point), they have  $\chi^2 = 439.1$  and 1107.6 with TOA rms of 0.041 s and 0.099 s, respectively, while the third has  $\chi^2 = 18.7$  with a TOA rms of 0.010 s (all for 14 degrees of freedom).

The timing solution derived from the *Chandra* and *XMM-Newton* TOAs is presented in Table 2. As indicated by the value of  $\chi^2$ , the data are well reproduced by simple spin-down; the addition of a cubic ( $\ddot{\nu}$ ) term leads to only an insignificant reduction in  $\chi^2$ , from 18.7 to 18.6, and the inferred value of  $\ddot{\nu} = -7(15) \times 10^{-26}$  Hz s $^{-2}$  is consistent with zero.

Unlike the *Chandra* and *XMM-Newton* data, however,

TABLE 2  
MEASURED AND DERIVED TIMING PARAMETERS FOR  
RX J1308.6+2127 FROM *Chandra* AND *XMM-Newton* DATA

Quantity <sup>a</sup>	Value
Dates (MJD) .....	51720–53581
$t_0$ (MJD) .....	53415.687853(2)
$\nu$ (Hz) .....	0.0969694896(2)
$\dot{\nu}$ (Hz s $^{-1}$ ) .....	$-1.053(3) \times 10^{-15}$
TOA rms (s) .....	0.010
$\chi^2/\text{DOF}$ .....	18.7/14=1.34
$P$ (s) .....	10.31252206(2)
$\dot{P}$ (s s $^{-1}$ ) .....	$1.120(3) \times 10^{-13}$
$\dot{E}$ (erg s $^{-1}$ ) .....	$4.0 \times 10^{30}$
$B_{\text{dip}}$ (G) .....	$3.4 \times 10^{13}$
$\tau_{\text{char}}$ (yr) .....	$1.5 \times 10^6$

NOTE. — Uncertainties quoted are twice the formal  $1-\sigma$  uncertainties in the fit.

the *ROSAT* HRI point is slightly discrepant from the fit in Table 2, exceeding it by 0.15(3) cycles. If we include it in the fit, the overall solution does not change drastically ( $\dot{\nu}$  becomes  $-1.050(2) \times 10^{-15}$  Hz s $^{-1}$ ) and the deviation does decrease to 0.11(3) cycles, but the overall  $\chi^2$  increases to 43.5 for 15 degrees of freedom (with a TOA rms of 0.0271 s). The deviation could be intrinsic (a glitch, timing noise, precession, changes in pulse profile), but might also be instrumental, perhaps related to differences in energy responses between the different instruments. Unfortunately, the sampling is too sparse to determine a unique solution. As an example, we show in Figure 2 a cubic fit that matches the HRI point reasonably well, with  $\chi^2 = 22.5$  for 14 degrees of freedom, TOA rms of 0.011 s, and  $\ddot{\nu} = -2.5(5) \times 10^{-25}$  Hz s $^{-2}$ . We stress, however, that, in essence, this solution approximates the *Chandra* and *XMM-Newton* data with a  $\ddot{\nu} = 0$  model and then adjusts  $\dot{\nu}$  to pass through the HRI point. Hence, it does not give much additional insight.

#### 4. DISCUSSION & CONCLUSIONS

The spin period and spin-down rate we derive for RX J1308.6+2127 are quite similar to those of RX J0720.4–3125, the only other isolated neutron star with a timing solution (Kaplan & van Kerkwijk 2005), placing both of them above the pulsar “death-line” in a  $P$ - $\dot{P}$  diagram despite their lack of radio emission (Kaplan et al. 2002a, 2003). Hence, assuming both spin down by magnetic dipole radiation, RX J1308.6+2127 and RX J0720.4–3125 have similar inferred magnetic field strengths ( $B_{\text{dip}} = 3.4$  and  $2.4 \times 10^{13}$  G, respectively), characteristic ages ( $\tau_{\text{char}} = 1.5$  and 1.9 Myr), and spin-down luminosities ( $\dot{E} = 4.0$  and  $4.7 \times 10^{30}$  ergs s $^{-1}$ ). Both sources also have thermal X-ray spectra with temperatures of  $\sim 1 \times 10^6$  K, but superposed on these are rather different absorption features: in RX J1308.6+2127, the absorption feature is centered near or below 300 eV and is very wide and strong, with an equivalent width of  $> 150$  eV (Haberl et al. 2003); in RX J0720.4–3125, on the other hand, no absorption was apparent until 2004, when an absorption feature with only a slightly higher energy but much smaller equivalent width ( $\sim 40$  eV) appeared (Haberl et al. 2004; de Vries et al. 2004). If the magnetic fields, line energies,

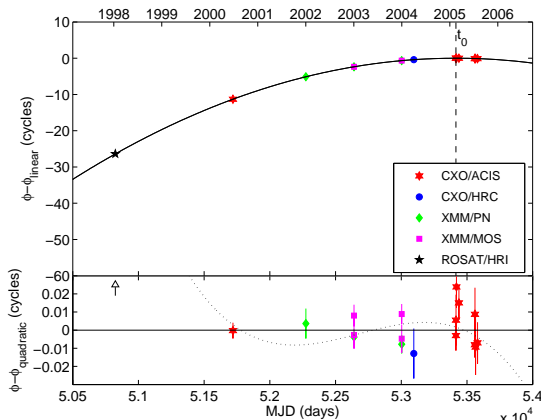


FIG. 2.— Phase residuals for RX J1308.6+2127. The top panel shows the residuals for each TOA compared to a linear ( $\dot{\nu} = 0$ ) model. The solid curve gives the best-fit quadratic ( $\dot{\nu} \neq 0, \ddot{\nu} = 0$ ) ephemeris for all the *Chandra* and *XMM-Newton* data (Tab. 2). The vertical dashed line indicates the reference time  $t_0$ . The bottom panel shows the residuals relative to the quadratic model; the *ROSAT* HRI point is off the scale at 0.14 cycles, and so is indicated with an arrow in this panel. We also show a best-fit cubic model fitted to all of the data including the *ROSAT* point ( $\dot{\nu} \neq 0$ ; dotted line).

and blackbody temperatures are all similar, what would account for the significant difference in line strength?

The interpretation of the absorption lines is still a matter of debate. For RX J1308.6+2127, Haberl et al. (2003) suggested proton cyclotron absorption in a field of  $(2\text{--}6) \times 10^{13}$  G, which could match both the energy and strength of the observed feature (for a gravitational redshift of  $z = 0.3$ , the observed line energy would be at 100–300 eV). As the feature in RX J0720.4–3125 was so much weaker but at a similar energy, van Kerkwijk et al. (2004) argued that for that source the proton cyclotron line was below the observed band and that the absorption was due to the  $0 \rightarrow 2$  transition between tightly-bound states of neutral hydrogen in a  $\sim 2 \times 10^{13}$  G field.

Qualitatively, the field strengths inferred from our timing measurements agree with the above expectations: the field of RX J1308.6+2127 is stronger than that of RX J0720.4–3125, while a weaker field would be expected if the absorption in both sources were due to the same mechanism. Quantitatively, a larger difference between the two sources was expected. However, this discrepancy may simply reflect orientation and/or substructure in the magnetic field—higher-order multipoles near the surface would affect the emission properties but not the spin-down rate. Such effects may also be responsible for the difference in pulse profile: double-peaked for RX J1308.6+2127, and sinusoidal for RX J0720.4–3125. Phase-resolved X-ray spectroscopy coupled with observations of more sources are probably the best ways to disentangle these effects, and efforts are underway (e.g., Haberl et al. 2004; Schwope et al. 2005).

Another open issue is that the characteristic ages of RX J0720.4–3125 and now RX J1308.6+2127 are three to four times larger than the values of  $\sim 0.5$  Myr one would expect for simple cooling models (Heyl & Hernquist 1998; Kaplan et al. 2002b; Zane et al. 2002) and, in the case of RX J0720.4–3125, tracing the object back along its trajectory to a likely birth location (Motch, Zavlin, & Haberl 2003; Kaplan 2004). Indeed,

this age discrepancy may extend to the other isolated neutron stars discovered by *ROSAT*: all have similar temperatures and thus likely similar cooling ages, and most also have similar periods (3–10 s) and, based on the similar energies at which they show X-ray absorption features (0.3–0.7 keV), similar magnetic field strengths, implying similar characteristic ages.

We first consider whether the discrepancy could result from the characteristic age being an overestimate. In general, for a spin-down torque  $\propto \nu^n$ , the pulsar's spin-down age is given by  $t_{\text{sd}} = [P/(n-1)\dot{P}] [1 - (P_0/P)^{n-1}]$ , where  $P_0$  is the initial spin period and  $n = \nu\ddot{\nu}/\dot{\nu}^2$  is the “braking index,” equal to 3 under the assumption of magnetic dipole radiation (e.g., Manchester & Taylor 1977, p. 111). For  $P_0 \ll P$  and  $n = 3$ , one recovers the characteristic age  $\tau_{\text{char}} \equiv P/2\dot{P}$ , but if  $P_0$  is not much smaller than the current period  $P$ , the characteristic age is an overestimate. While we cannot exclude the required birth periods of 7–8 s, there is as yet no concrete indication that neutron stars are born with periods longer than 100 ms (e.g., Kaspi & Helfand 2002; Gotthelf et al. 2005).

For RX J0720.4–3125, this led us to discuss the possibility that the neutron star formed in a binary system and accreted matter before being ejected in a second supernova; at ejection, the neutron star would still be hot from the accretion, but spinning slowly (Kaplan & van Kerkwijk 2005). A variation on this model would involve accretion from a residual debris disk such as that recently discovered around the anomalous X-ray pulsar 4U 0142+61 (Wang, Chakrabarty, & Kaplan 2005), but this assumes that the accretion disk persists for a sufficient time and can affect the spin-down of the neutron stars, both of which are far from clear. In either case, if accretion played a role, it might explain why the spectral properties of the isolated neutron stars are rather different from those of the radio pulsar population.

Unfortunately, the above solution for the age discrepancy is not unique. First, it is possible that the spin-down was not due to a constant dipole but that the magnetic field decayed (effectively, this implies  $n > 3$ ). Second, the cooling age could be incorrect due to non-standard cooling. For instance, the energy released by magnetic field decay might keep a neutron star hotter (Heyl & Kulkarni 1998; note, however, that these authors do not expect significant effects for the field strengths we infer) and longer cooling times are also expected for a light neutron star (Yakovlev et al. 2004). A prolonged cooling timescale seems somewhat unlikely in light of the kinematic age estimates, though it should be kept in mind that these may also not be unique: for RX J0720.4–3125, several different birth places are possible (Motch et al. 2003; Kaplan 2004).

Finally, when fitted with just a simple spin-down model, RX J0720.4–3125 showed significant timing residuals of 0.31 s (root-mean-square), much larger than the uncertainties on the TOAs. In contrast, for RX J1308.6+2127 the root-mean-square residuals are only 0.010 s (excluding the HRI point), consistent with measurement errors. Since the sources were observed with the same instruments, and have similar spectral shapes, the differences in timing behaviors are likely not instrumental. Instead, they may well reflect the fact that

both the spectrum and pulse profile of RX J0720.4–3125 are varying with time (de Vries et al. 2004; Vink et al. 2004), while RX J1308.6+2127 appears to be stable.

We acknowledge support through Chandra grant GO5-6050A.

## REFERENCES

Buccheri, R. et al. 1983, A&A, 128, 245

Cox, A. N. 2000, Allen's Astrophysical Quantities, 4th edn. (New York: AIP)

Davis, W., Holmes, J., & Myers, R. 2003, in Proc. 2003 Chandra Calibration Workshop (Cambridge: CXC), [http://cxc.harvard.edu/ccw/proceedings/03\\_proc](http://cxc.harvard.edu/ccw/proceedings/03_proc)

de Vries, C. P., Vink, J., Méndez, M., & Verbunt, F. 2004, A&A, 415, L31

Garmire, G. P., Bautz, M. W., Ford, P. G., Nousek, J. A., & Ricker, G. R. 2003, Proc. SPIE, 4851, 28

Gotthelf, E. V., Halpern, J. P., & Seward, F. D. 2005, ApJ, 627, 390

Haberl, F. 2004, Advances in Space Research, 33, 638, (astro-ph/0302540)

Haberl, F., Schwope, A. D., Hambaryan, V., Hasinger, G., & Motch, C. 2003, A&A, 403, L19

Haberl, F., Zavlin, V. E., Trümper, J., & Burwitz, V. 2004, A&A, 419, 1077

Hambaryan, V., Hasinger, G., Schwope, A. D., & Schulz, N. S. 2002, A&A, 381, 98

Heyl, J. S. & Hernquist, L. 1998, MNRAS, 297, L69

Heyl, J. S. & Kulkarni, S. R. 1998, ApJ, 506, L61

Kaplan, D. L. 2004, Ph.D. Thesis, California Institute of Technology

Kaplan, D. L., Kulkarni, S. R., & van Kerkwijk, M. H. 2002a, ApJ, 579, L29

Kaplan, D. L., Kulkarni, S. R., van Kerkwijk, M. H., & Marshall, H. L. 2002b, ApJ, 570, L79

Kaplan, D. L. & van Kerkwijk, M. H. 2005, ApJ, 628, L45

Kaplan, D. L., van Kerkwijk, M. H., Marshall, H. L., Jacoby, B. A., Kulkarni, S. R., & Frail, D. A. 2003, ApJ, 590, 1008

Kaspi, V. M. & Helfand, D. J. 2002, in ASP Conf. Ser. 271: Neutron Stars in Supernova Remnants, ed. P. O. Slane & B. M. Gaensler (San Francisco: ASP), 3, (astro-ph/0201183)

Kraft, R. P. et al. 1997, Proc. SPIE, 3114, 53

Manchester, R. N. & Taylor, J. H. 1977, Pulsars (San Francisco : W. H. Freeman, c1977.)

Motch, C., Zavlin, V. E., & Haberl, F. 2003, A&A, 408, 323

Schwope, A. D., Hambaryan, V., Haberl, F., & Motch, C. 2005, A&A, 441, 597

Schwope, A. D., Hasinger, G., Schwarz, R., Haberl, F., & Schmidt, M. 1999, A&A, 341, L51

Strüder, L. et al. 2001, A&A, 365, L18

Turner, M. J. L. et al. 2001, A&A, 365, L27

van Kerkwijk, M. H., Kaplan, D. L., Durant, M., Kulkarni, S. R., & Paerels, F. 2004, ApJ, 608, 432

Vink, J., de Vries, C. P., Méndez, M., & Verbunt, F. 2004, ApJ, 609, L75

Wang, Z., Chakrabarty, D., & Kaplan, D. L. 2005, Nature, in press

Yakovlev, D. G., Gnedin, O. Y., Kaminker, A. D., Levenfish, K. P., & Potekhin, A. Y. 2004, Advances in Space Research, 33, 523, (astro-ph/0306143)

Zane, S., Haberl, F., Cropper, M., Zavlin, V. E., Lumb, D., Sembay, S., & Motch, C. 2002, MNRAS, 334, 345

Zombeck, M. V., David, L. P., Harnden, F. R., & Kearns, K. 1995, Proc. SPIE, 2518, 304